Acoustic eigenanalysis of 2D open cavity with Vekua approximations and the method of particular solutions

Alexandre Leblanc, Gilles Chardon

Acoustic eigenanalysis of 2D open cavity with Vekua approximations and the Method of Particular Solutions

Alexandre Leblanc[a,*], Gilles Chardon[b]

[a] *Univ Lille Nord de France, F-59000 Lille, France*
UArtois, LGCgE, F-62400 Béthune, France
[b] *Austrian Academy of Sciences, Wohllebengasse 12-14, 1040 Wien, Austria*

Abstract

This paper discusses the efficient extraction of acoustic resonances in 2D open cavities using a meshless method, the method of particular solutions. A first order, local non-reflecting boundary condition is chosen to account for the opening and Fourier-Bessel functions are employed to approximate the pressure at the borders of the cavity and inside. A minimization problem is then solved for the complex frequency range of interest. For the investigated cavity, the minimum values obtained match those found in previous published studies or by other numerical methods. But, unlike the perfectly matched layer absorbing boundary conditions now usually employed, this approach is free from spurious eigenfrequencies. Moreover, the specific treatments of the geometric singularities allow this method to be particularly efficient in the presence of corner singularities.

Keywords: eigenanalysis, meshless method, Vekua theory

Introduction

Acoustic resonances of open cavities are crucial in many industrial, aeronautical or marine applications. For transport, noise due to open cavities is omnipresent: open windows for cars [1], intercoach gaps for trains [2] or landing gear traps for planes [3]. Acoustic characterization of urban environments and streets is another field of active research, as the sound propagation

*Corresponding author
Email address: alexandre.leblanc@univ-artois.fr (Alexandre Leblanc)

is often treated through an open waveguide [4]. Beyond noise considerations, musical acoustics is also concerned in studying these resonances, especially for the design of wind or string instruments. The last decades have brought a deep understanding of the mechanisms behind the noise produced by the interaction of an air flow with an open cavity [3, 5], but the suppression, or at least the significant reduction of the feedback loop of this coupling is still challenging [5]. Active control techniques are the most promising answers [6], but a critical issue for those tools is the location of the secondary sources and error sensor [7]. Indeed, nodal lines must be avoided in order to have an efficient noise control on each acoustic mode of interest. Moreover, knowing the frequencies of these resonances at the design phase is also necessary if implementing effective passive control techniques. Often, the task can be reduced to the determination of acoustic resonances of the open cavity without flow. Indeed, the acoustic cavity tones generated are practically independent of the velocity flow at low Mach numbers.

Eigenanalysis of cavities can be treated in numerous ways. In the cases of simple geometries, analytic solutions are likely to be obtained at low computational cost and high precision (according to the possible simplifications made on the real geometry). The effective resonances can be also obtained through an experimental setup, which is prone to give by definition relevant answers, but often comes with prohibitive cost and with only minimum quantitative information. So, a good addition (nowadays, it even tends to be a replacement) is to build and solve numerical models, sufficiently representative of the physics involved here. These models are based on numerical techniques such as, and for the most part, the finite element method (FEM). However, it can be computationally intensive at high frequencies or in the presence of singularities (e.g. corner singularities). Alternative methods have emerged to lower this shortcoming, one can cite the boundary element method (BEM) and meshless methods as the method of fundamental solutions (MFS). Unfortunately, these methods come with other difficulties, leaving, decades after decades, the FEM as the routine tool for most of acoustic studies. So, it is no surprise that the majority of attempts for performing the numerical eigenanalysis of open cavities is based on a similar approach to that of Koch [8], who solved the Helmholtz wave equation by FEM, and using a perfectly matched layer (PML). The main idea is to cover the original open cavity by another fluid domain, bounded by a baffle in the extension of the opening and otherwise, by a non-reflecting boundary (feature brought by the PML). While robust, this approach exhibits the major

drawback of introducing spurious modes in the solution spectrum, in addition to be sometimes high-demanding from a computational point of view. Indeed, automatic distinction between artificial (PML domain) and relevant eigenvalues (cavity) remains challenging. Before the advent of PML, two approaches have been widely developed in order to avoid nonphysical reflections at artificial boundaries (those that allow the truncation of physical domain). The first set of these non-reflecting boundary conditions (NRBC) brings local relation between the pressure and its derivative, while the other family is an exact NRBC known as Dirichlet-to-Neumann (DtN) map [9]. The merits and drawbacks of these different approaches have been thoroughly discussed by Givoli [10] and Tsynkov [11]. These authors state that none is clearly superior to others, and that the choice should be based on arbitrary constraints (robustness, ease of implementation or computational efficiency).

In this paper, eigenanalysis of 2D open cavities by the method of particular solutions (MPS) with local NRBC is discussed. The MPS is dedicated to the eigenanalysis of elliptic operators and was originally proposed by Fox, Henrici and Moller [12]. It has generated as much enthusiasm (for its simplicity) as disappointment: while efficient for simple geometries, stability problems arise for more complicated domains. Recently, Betcke and Trefethen [13] proved that these failures are due to a single cause: the original MPS does not impose nonzero eigenfunctions. With the introduction of interior collocation points, Betcke and Trefethen circumvent this issue, substituting the determinant computation in [12] by the resolution of a generalized eigenvalue problem. Now a robust method, the MPS offers some advantages in the present context: the formulation is straightforward, consistent with local ABC, and multiple eigenvalues are easy to determine, with the associated eigenspaces readily recovered.

This algorithm needs an approximation scheme for the solutions to the considered partial differential equation. In [12, 13], fractional Fourier-Bessel functions were used, while Fourier-Bessel and modified Fourier-Bessel were employed in [14] to treat the case of Kirchhoff-Helmholtz plates. The approximation given by the MFS could also be used (note here that the MPS is a *computational* method, i.e. an algorithm, while the MFS is an *approximation* method). However the approximation schemes usually used in conjonction with the MPS are free from any spurious modes [13], unlike the MFS [15].

In order to take into account the cavity opening, local NRBC are considered here, linking only nearby neighbors of a boundary point. For the wave equation, Bayliss *et al.* [16] constructed a sequence of ABC based on

the asymptotic expansion of the solution to the exterior Helmholtz equation. Since the condition is written in polar coordinates, it is most convenient when the virtual boundary is a circle. Li and Cendes [17] proposed a similar NRBC using the full convergent expansion of the solution (see Medvinsky [18] for the link between both formulations). While the Bayliss NRBC is best known, the Li–Cendes form is expected to be more efficient if the non-reflecting boundary is close to the scatterer, which is the case in the present context.

The layout of the paper is as follows. Section 1 presents the computational model leading to the approximation of open cavity eigenmodes. To this end, local non-reflecting boundary conditions, the method of particular solution and the Vekua theory are briefly recalled. Numerical results are presented in section 2 and are also compared with solutions obtained by the FEM with PML [8]. Finally, the main conclusions are outlined in section 3.

1. Eigenmodes of an open cavity

An acoustic open cavity filled with fluid in a semi-infinite wall is considered, as sketched in Fig. 1. The problem of interest consists of the iden-

Figure 1: Rectangular open cavity

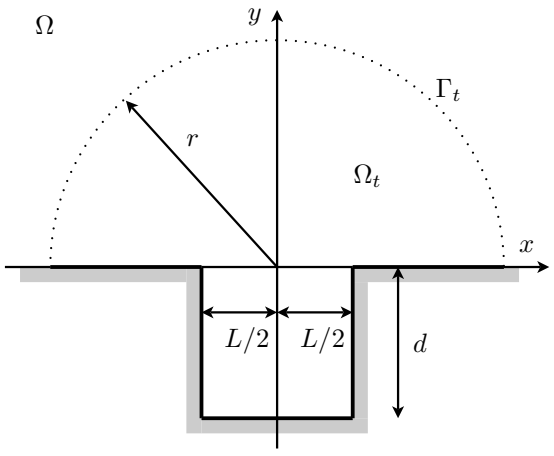

tification of the eigenmodes of this cavity. This problem is defined in the unbounded domain Ω by the Helmholtz equation and its boundary condi-

tions as

$$\Delta u + k^2 u = 0 \quad \text{in } \Omega \tag{1}$$

$$\frac{\partial u}{\partial n} = 0 \quad \text{on } \Gamma \tag{2}$$

$$\lim_{r\to\infty} r^{1/2}\left(u_r - iku\right) = 0 \quad \text{uniformly in } \theta \tag{3}$$

The pressure amplitude u exhibits an implicit $e^{-i\omega t}$ time dependence, with ω is the circular frequency. $k = \omega/c$ is the wave number assuming c the wave speed in Ω. The boundary condition for the opening is the Sommerfeld radiation condition, which dictates that waves are outgoing. In order to reformulate the problem on a bounded domain, this condition must be replaced by a boundary operator B, applied on an artificial boundary Γ^t (here, a half circle): Eq. (3) is replaced by $Bu = 0$ on Γ^t and Eq. (1) is now limited to Ω^t, which is the domain resulting from the truncation of the unbounded domain Ω by the artificial boundary Γ^t. An exact NRBC is the Dirichlet-to-Neumann map [9]. This non-local boundary condition is robust, accurate, stable and in the context of FEM, leads to a well-conditioned (but no longer sparse) matrix problem. However, getting the expression of the DtN condition is not a trivial task and can be too complicated to be practical. In order to have the widest scope of use, we restrict our attention to local NRBCs.

1.1. Local non-reflecting boundary conditions

The first successful construction of local NRBCs is credited to Engquist and Majda [19], using rational functions approximation of the pseudo-differential operator accounting for the exact boundary condition. Such approach is equivalent to a one-way equation, that only allows propagation from the interior to the exterior [20]. Similar property is obtained if using a circular artificial boundary, with the annihilation of leading terms in the asymptotic [16] or modal [17] expansion of the solution in the far field. All sequences of these local NRBCs can be written in the form

$$\frac{\partial u}{\partial r} = -L_K u \quad \text{on } \Gamma^t \tag{4}$$

Using first-order NRBCs for a circular boundary of radius R, L_K could be defined as

$$L_K = \begin{cases} ik + \frac{1}{2R}, & \text{Bayliss} \\ k\frac{H_1(kR)}{H_0(kR)}, & \text{Li–Cendes} \end{cases} \tag{5}$$

where $H_n(kR)$ are Hankel functions. The Li–Cendes expansion is used in this paper, since only the low-frequency spectrum (where the asymptotic expansion of Bayliss is expected to be less efficient [21]) is of particular concern here.

1.2. The method of particular solutions

The basic idea behind the MPS is to consider separately the spaces of solutions of the Helmholtz equation for different wave numbers. In each solution spaces, a nonzero function satisfying the boundary conditions is then an eigenmode. As originally formulated for Dirichlet boundary conditions, the MPS needs N points x_j on the border of the domain, associated with N functions ϕ_i spanning a subspace which approximates the set of solutions to the Helmholtz equation with a given wavenumber k. In order to obtain the eigenfrequencies, a square matrix $M(k)$ containing the values of ϕ at the N points is build and its determinant computed:

$$\det(M(k)) = \begin{vmatrix} \phi_1(x_1) & \cdots & \phi_N(x_1) \\ \vdots & & \vdots \\ \phi_1(x_N) & \cdots & \phi_N(x_N) \end{vmatrix} \tag{6}$$

If a linear combination of functions is zero on the border, then the determinant is zero. As only a finite dimensional-space is considered, the boundary condition is unlikely to be exactly satisfied, and the eigenfrequencies are obtained as the local minima of this determinant. As pointed out by Betcke and Trefethen [13], this simple method has limitations. First, the discretization of the solutions space and boundaries sampling must be of equal size. Second, $M(k)$ gets ill-conditioned as the number of functions grows. To avoid these problems, the same authors suggest to solve the following optimization problem:

$$\tau(k) = \min_u \|Tu\|^2_{L^2(\partial\Omega)} \tag{7}$$

under the constraints that $\|u\|^2_{L^2(\partial\Omega)} = 1$ and that u is solution to the Helmholtz equation, and where T is the trace operator on the boundary $\partial\Omega$. If the tension $\tau(k)$ is zero, then there is a nonzero function in Ω that is zero on its boundary, and k is an eigenfrequency. For a family of functions (ϕ_i) chosen for the approximation of the solutions of the Helmholtz equation with wavenumber k, and with expansion coefficients $\mathbf{u} = (u_1, \ldots, u_N)$, we

have

$$u = \sum_{n=1}^{N} u_n \phi_n$$
$$\|Tu\|^2_{L^2(\partial\Omega)} = \mathbf{u}^* \mathbf{F} \mathbf{u}$$
$$\|u\|^2_{L^2(\Omega)} = \mathbf{u}^* \mathbf{G} \mathbf{u}$$

where the coefficients of the matrices $\mathbf{F}$ and $\mathbf{G}$ are

$$F_{ij} = \langle T\phi_i, T\phi_j \rangle_{L^2(\partial\Omega)}$$
$$G_{ij} = \langle \phi_i, \phi_j \rangle_{L^2(\Omega)}$$

Here, the optimization problem (7) is replaced by a generalized eigenproblem

$$\lambda \mathbf{F} \mathbf{u} = \mathbf{G} \mathbf{u} \tag{8}$$

whose largest eigenvalue is the inverse of $\tau(k)$ [13]. For an eigenvalue k, the eigenvector $\mathbf{u}$ corresponding to the largest eigenvalue contains the expansion coefficients of the associated eigenmode. Since the matrices $\mathbf{F}$ and $\mathbf{G}$ depend on k, the computation of $\tau(k)$ necessitates to solve (8) for a large number of possible wavenumbers k. However, the size of these generalized eigenvalue problems is small compared to the size of the matrices involved in, e.g., the FEM. Here, only the largest eigenvalue is needed, and the particular behavior of $\tau(k)$ (see Figs. 2 and 3 or Fig. 9.3 in [13]) could also be used to design a more efficient search of the minimas of $\tau(k)$.

In practice, the matrices $\mathbf{F}$ and $\mathbf{G}$ have to be numerically evaluated. This can be done by numerical quadrature (gaussian, Monte-Carlo, etc.). It is worth noting that it is not critical to have an accurate estimation of the L_2 norms on the border and interior of Ω as their actual values are not used by the method: the objective is to obtain a null border norm with a non-zero interior norm.

While here introduced for the Helmholtz equation and Dirichlet boundary conditions, this method can be applied to more general cases, such as the eigenanalysis of plates [14], by using the appropriate approximation scheme and boundary conditions.

1.3. The Vekua theory for the Helmholtz equation

In its general formulation, the Vekua theory [22, 23] gives approximations of solutions to general elliptic partial differential equations, by building

invertible operators mapping these solutions to harmonic functions. The particular case of the Helmholtz equation in 2 and 3 dimensions has been analyzed by Moiola *et al.* [24]. The salient result of this study is that the solution of Eq. (1) can be approximated, on a star-shaped domain, by generalized harmonic polynomials, *i.e.* functions of the form

$$u_K = \sum_{j=-K}^{K} c_j J_j\left(kr\right) e^{in\theta} \tag{9}$$

where (r, θ) is the polar coordinates system and c a weighting vector. In the context of the MPS, the Vekua theory allows to choose a family of functions perfectly suited to the approximation of the Helmholtz equation solutions.

As shown in [24], the approximation error can be bounded, in Sobolev norms, by

$$\|u - u_K\|_{H^q} \leq C \left(\frac{\ln K}{K}\right)^{p-q} \|u\|_{H^p}. \tag{10}$$

with p and q integers such that $p > q$. When the function to be approximated has singularities, the convergence is slowed down. Such singularities usually appear at singular corners of the domain, i.e corners with angle π/α with $\alpha \notin \mathbb{N}$. To deal with such cases, it is possible to add fractional Fourier–Bessel functions to capture these singularities and accelerate the convergence [13, 25]. The particular form of these functions depends on the boundary conditions. We have here Neumann boundary conditions on the boundary of the domains, and use, near a corner of angle π/α, fractional Fourier–Bessel functions defined by:

$$u^{(n)}\left(\rho, \psi\right) = J_{\alpha n}\left(k\rho\right) \cos \alpha n \psi \tag{11}$$

with $n \in \mathbb{N}^\star$, in local coordinates (ρ, ψ) centered at the corner and one of its edges as the origin of the angle ψ. In presence of N_c singulars corners with angles π/α_l, the solutions to the Helmholtz equation are approximated by linear combinations of Fourier–Bessel functions of the form

$$\sum_{j=-K}^{K} c_j J_j\left(kr\right) e^{in\theta} + \sum_{l=1}^{N_c} \sum_{j=1}^{K_l} c_j^l J_{\alpha_l j}\left(k\rho_l\right) \cos(\alpha_l j \psi_l) \tag{12}$$

with (ρ_l, ψ_l) polar coordinates with respect to the l-th corner. The fractional Fourier–Bessel functions capture the singularities at the corners, leaving a

residual that is more regular than the original function, allowing a faster convergence of the approximation by regular Fourier–Bessel functions, as indicated by (10).

1.4. Approximation of open cavity eigenmodes

The results and techniques discussed above are now pieced together to yield a numerical method to compute eigenmodes of open cavities.

We approximate the solutions to the Helmholtz equation on the domain Ω_t, assumed to be star-shaped, with Fourier–Bessel function. As the domain is likely to have singular corners, e.g. at the junction of the cavity with the baffle, we add fractional Fourier–Bessel functions to the family of functions. The boundary conditions are Neumann boundary conditions on Γ and the local NRBC given by Eq. (5). The corresponding tension is then

$$t = \int_{\Gamma} \left| \frac{\partial u}{\partial n} \right|^2 + \int_{\Gamma_t} \left| \frac{\partial u}{\partial n} + L_K u \right|^2 \tag{13}$$

where u is here approximated by the Fourier–Bessel functions of the previous section. For each frequency, the goal is to compute the set of c_n leading to lowest value of t. The complex eigenfrequencies are the local minimas of the tension. It is worth noting that the condition number of the matrix defining the tension is stable when evaluated at the sought eigenvalues.

2. Numerical results

In the following investigations, the Fourier-Bessel functions are centered at the origin, which is also the center of the circular NRBC. While the domain is not necessarily star-shaped with respect to a disk around this center, and the results by Moiola et al. not directly applicable, it is shown in the appendix that the choice of the center has no incidence on the approximation rate. For the treatment of the singularities which can arise at corners of the studied domains, fractional Fourier-Bessel are used, centered on these corners [13, 25].

The first investigation deals with the square open cavity. This case is the same that the one depicted in Fig. 2b of Koch's paper [8]. Figure 2 compares the results obtained with the present MPS formulation, using $K = 32$ Fourier–Bessel functions and 40 expansions terms for the opening corners (cf. Eq. 11), with those of Koch (FEM with PML). Here, L_k is the first-order Li–Cendes NRBC with $R = L/2$. The cavity is discretized with 58

equally spaced boundary nodes and 100 nodes on the NRBS boundary to estimate the coefficients of the matrix $\mathbf{F}$, and 100 nodes inside the cavity for $\mathbf{G}$. Overall, the eigenmodes found with the present approach coincide well

Figure 2: Open square cavity resonances: color field is $(1/t)$ on a decibel scale (dB) using Li–Cendes NRBC (with $R = L/2$), the 'o' marks are the values obtained by Koch [8] [Fig. 2b]

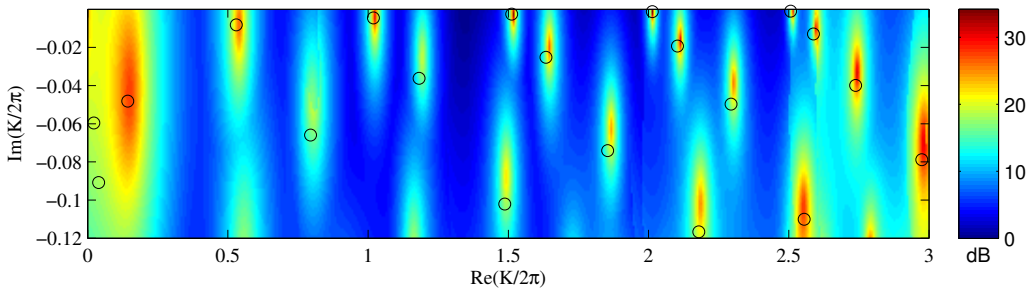

with those found in [8]. The two first values very close to the imaginary axis are missing with the MPS as they are due to the discrete approximation of the continuous spectrum by the PML boundaries. Also, it is worth noting that the additional PML modes polluting the solution are not shown here, as in [4, 8]. These eigenvalues, only linked to the PML parameters, are filtered out thanks to their corresponding eigenmodes but at the cost of a post-processing analysis, which can be time consuming. Such procedure is completely avoided using the MPS approach. For the weakly damped eigenvalues (the physically dominant modes), the difference between the two calculations are low. The discrepancies for the higher damped modes are due for the most part to the location of the NRBC, being in the near-field. These differences may also be linked to the treatment of the cavity opening corners (eg. the number of expansion terms used) when Γ does not include the semi-infinite wall. Figure 3 compares the results between three approaches for an identical domain Ω_f ($R = 2L$). The 58 additional nodes discretizing the wall further enhance the MPS efficiency. Indeed, and in addition to better results for the most damped modes, a better contrast is obtained, which may be crucial to identify close spaced eigenfrequencies. Raw results for a FEM simulation (12366 triangular elements) with Li–Cendes NRBC are also shown in Fig. 3. The MPS clearly benefits of the specific treatment of the opening corners. Perhaps more importantly, the MPS proves to be free from spurious eigenvalues, those linked to the half-disk above the open cavity, as

small eigenfunctions on boundary points automatically enforce unit norms at interior points [13]. These examples demonstrate the ability of the MPS

Figure 3: Open square cavity resonances using Li–Cendes NRBC (with $R = 2L$): color field is the MPS results, dots are the values obtained with a FEM solver. The 'o' marks are the values obtained by Koch [8] [Fig 2b]

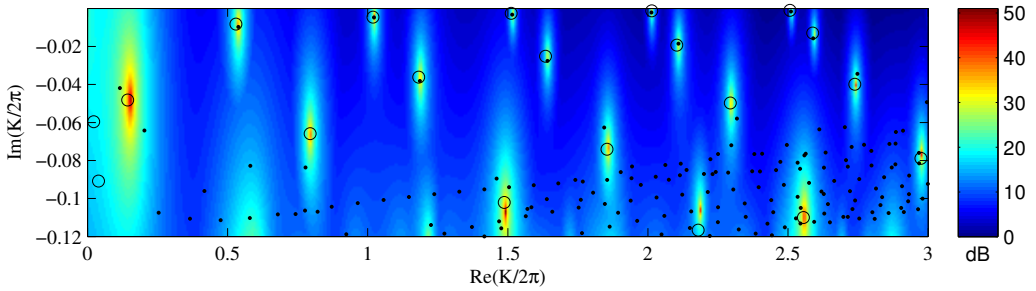

to efficiently perform the eigenanalysis of open cavities.

We now investigate implementation issues, such as the influence of the ratio R/L, the choice of the sampling points and the approximation order on the accuracy.

Using Li–Cendes NRBC as defined by Eq. (5), its sole parameter is the choice for R. Figure 4 shows the variation of the 18 first eigenfrequencies with R. The position of the eigenfrequencies appears to be stable whatever

Figure 4: Variation of resonant frequencies with the NRBC radius R

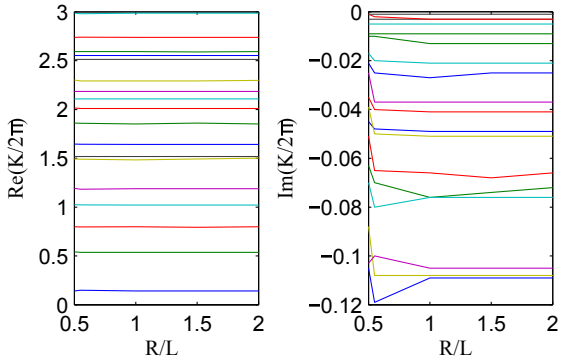

the choice of R whereas the damped part is clearly sensitive to the inclusion of nodes linked to the semi-infinite wall. With the higher contrast obtained in such cases (cf. Fig. 3), adding few nodes of the rigid baffle in the MPS (thus

leading to a somehow far-field NRBC) seems to be a necessity, especially considering the low numerical cost induced.

For the interior points, it seems at first legitimate to question the importance of their number and their position on the results. The answer which encompasses these two preoccupations is given by Betcke and Trefethen:

> A random distribution of interior points has always proved effective. In principle the method would fail if all points fell in regions where the eigenfunction is close to zero, but this is easily prevented by taking a healthy number of randomly distributed points. For the speed of the algorithm there is not much difference between 50 or 500 interior points

Indeed, these considerations are still valid for the eigenanalysis of open cavities as performed here. An example of the nodes/points repartition used for $R = d = 2L$ is illustrated by Fig. 5. Figure 6 shows the spectrum of reso-

Figure 5: Boundary nodes and interior points distribution

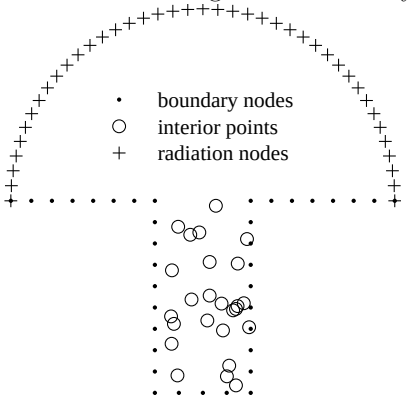

nances for the deep cavity case ($L/d = 0.5$). Also shown in this figure are the antisymmetric eigenfunctions $\phi(3, q)$ for $q = 0 \dots 7$ and can be compared to those of Fig. 6 in [4] (where $\phi(3, 6)$ is in fact $\phi(3, 7)$ as $\phi(3, 6) \approx 0.214 - i0.6$, cf. [8]). In order to illustrate the need for the specific treatment of the geometrical corners, the influence of the amount of fractional Fourier–Bessel functions is illustrated in Fig. 7. The tension, if function of the numbers of Fourier–Bessel (K) and fractional Fourier–Bessel (K^*) functions used, is plotted at the complex frequency corresponding to the modes $\phi(3, 0)$ and $\phi(3, 4)$. With no fractional Fourier–Bessel functions, the approximation provided by the Fourier–Bessel functions is highly singular, and, as predicted

Figure 6: Samples eigenfunction obtained with MPS for a deep open cavity ($d = 2L$, see [4])

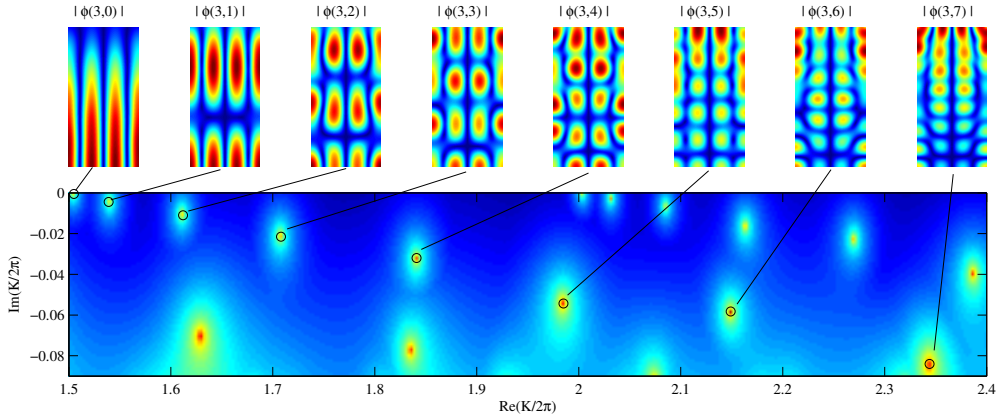

by Eq. (10), the convergence is very slow. Adding fractional Fourier–Bessel functions to the family used to approximate the Helmholtz solutions allows a much faster convergence, but as the estimated complex frequency is not *exactly* the true frequency, the tension still converges to a low, but nonzero, value. Being more general than the method depicted in [4], the present ap-

Figure 7: Influence of the number of fractional Fourier–Bessel functions used (K^*) for the determination of the antisymmetric modes $\phi(3,0)$ and $\phi(3,4)$ (cf. Fig. 6)

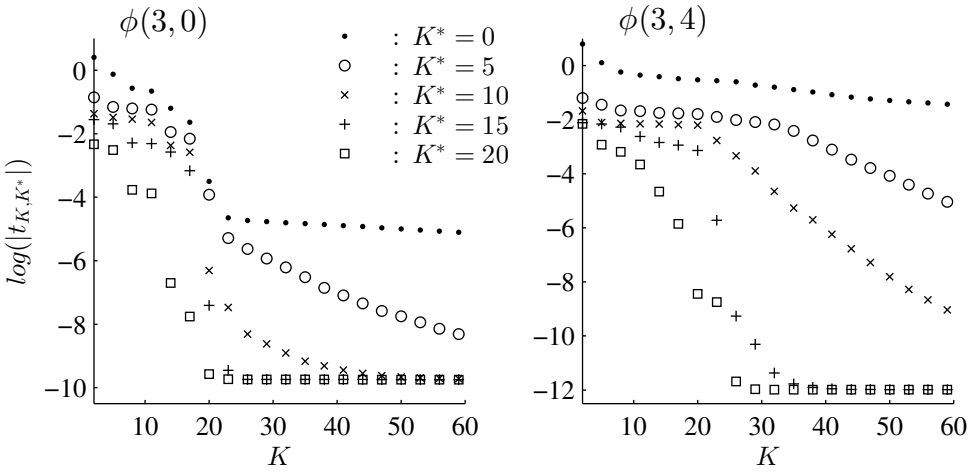

proach also leads to accurate determination of the eigenmodes when applied to arbitrary shaped open cavities (cf. Fig. 8). For this cavity, the four ge-

ometric singularities are handled with 32 Fourier–Bessel functions and the boundary is discretized with 72 nodes. The eigenfrequency and corresponding pressure pattern computed by the MPS and shown in Fig. 8 are close to those calculated with a commercial FEM solver (both methods using a Li–Cendes NRBC with $R = 2L$). For this last numerical experiment, converged eigenvalues are obtained using more than 5000 quadratic triangular elements, where the MPS solve a generalized eigenproblem of size 125.

Figure 8: Eigenfunction (absolute pressure) comparison between MPS and FEM, the cavity is open at its largest side

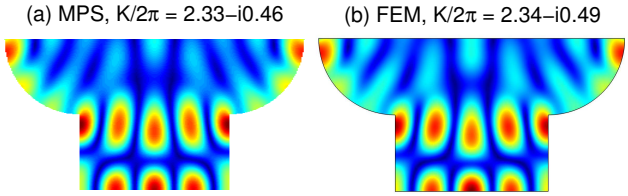

3. Conclusion

The method of particular solutions has been employed with a local non-reflecting boundary condition for the eigenmodes of open cavities. Following the Vekua theory for the Helmholtz equation, generalized harmonic polynomials are used to approximate the unknown pressure. The functions parameters are determined thanks to an optimization problem. In the case of a square cavity, this approach gives eigenvalues similar to those found by a FEM eigenanalysis. Fourier–Bessel functions of fractional orders at geometric singularities bring satisfying results even if the discretization is limited to the cavity. However, inserting few nodes of the exterior boundary (eg. the rigid baffle) improves both the accuracy and interpretation of results (higher contrast for the minimization problem, which may be essential in the case of closely spaced frequencies). A remarkable feature of this approach is that no spurious modes are produced, thanks to randomly located points inside the cavity. This gives this approach a real interest for numerical computations. For example, it can be used for the urban noise propagation, as performed in [4], with a more realistic street canyon geometry and without having to perform a tedious sorting between spurious and effective eigenmodes.

Appendix A. Approximation by decentered Fourier-Bessel functions

In [24], the Fourier-Bessel approximation for the solutions to the Helmholtz equation is proved when the domain Ω, on which the solutions are considered, is star-shaped with respect to a disk D of radius δ around the origin of the polar coordinates. Thus, in Sobolev norms:

$$\|u - u_N\|_{H^q(\Omega)} \leq C \left(\frac{\log N}{N} \right)^{p-q} \|u\|_{H^p(\Omega)}, \tag{A.1}$$

where

$$u_N = \sum_{n=-N}^{N} \alpha_n^N J_n(kr) e^{in\theta}. \tag{A.2}$$

We prove here that the rate of convergence is retained when the center of the polar coordinates is moved. Results on Bessel functions are available in [26, 27].

Using Graf's theorem, the origin of the Fourier-Bessel functions can be moved:

$$\begin{aligned} u_N = \sum_{n=-N}^{N} \alpha_n^N \sum_{m \in \mathbf{Z}} & J_{m+n}(kR) e^{i(n+m)\Theta} \\ & \times J_m(k\rho) e^{im\psi} \end{aligned} \tag{A.3}$$

where (ρ, ψ) are the polar coordinates with respect to the new center, of polar coordinates (R, Θ). Then, u can be approximated by:

$$\begin{aligned} \tilde{u}_N = \sum_{n=-N}^{N} \alpha_n^N \sum_{m=-3N-2}^{3N+2} & J_{m+n}(kR) e^{i(m+n)\Theta} \\ & \times J_m(k\rho) e^{im\psi}. \end{aligned} \tag{A.4}$$

For orders larger than $k\rho_m$, the Fourier-Bessel functions are increasing on $(0, \rho_m)$ (cf. [27] Eq. (A.4)), where ρ_m is the maximal distance between a point of Ω and the center of the polar coordinates. Thus, for $N > k\rho_m$, the

approximation error is:

$$|u_N - \tilde{u}_N| = \Bigg| \sum_{n=-N}^{N} \alpha_n^N \sum_{|m|>3N+2} J_{m+n}(kR) \times e^{i(n+m)\Theta} J_m(k\rho) e^{im\psi} \Bigg| \tag{A.5}$$

$$\leq \sum_{n=-N}^{N} |\alpha_n^N| \sum_{|m|>3N+2} |J_{m+n}(kR)| \times |J_m(k\rho_m)| \tag{A.6}$$

On the disk D, we have:

$$\int_D |\alpha_n^N J_n(kr)|^2 \leq \int_D |u_N|^2 \tag{A.7}$$

$$\leq \|u_N\|^2_{L^2(\Omega)} \tag{A.8}$$

as the Fourier–Bessel functions are orthogonal on the disk D. As $\|u_N\|_{L_2(\Omega)}$ converges to $\|u\|_{L_2(\Omega)}$, for high orders N we have $\|u_N\|_{L_2(\Omega)} \leq C\|u\|_{L_2(\Omega)}$ where C is a constant larger that 1. Using

$$\int_D |J_n(kr)|^2 = 2\sum_{l=0}^{\infty}(n+1+2l) J^2_{n+1+2l}(k\delta) \tag{A.9}$$

$$\geq J^2_{n+1}(k\delta), \tag{A.10}$$

gives a bound on α_n^N:

$$|\alpha_n^N| \leq \frac{C\|u\|_{L^2(\Omega)}}{J_{n+1}(k\delta)} \tag{A.11}$$

In the case where $J_{n+1}(k\delta)$ is zero for some n, a smaller δ' such that $J_{n+1}(k\delta') \neq 0$ for all n can be used. Note that in a given interval $(0, x)$, the Bessel functions have only a finite number of zeros as the Bessel functions J_n with $n > x$ are strictly positive (cf. [27] Eq. (A.4)) for $x > 0$. It is therefore always possible to find such a radius δ'.

The error between u_N and $\tilde{u}_N$ can be bounded by:

$$|u_N - \tilde{u}_N| \leq C \sum_{n=-N}^{N} \frac{\|u\|_{L^2(\Omega)}}{|J_{n+1}(k\delta)|} \times \sum_{|m|>3N+2} |J_{m+n}(kR)||J_m(k\rho_m)| \tag{A.12}$$

$$\leq (2N+1)C\|u\|_{L^2(\Omega)} \frac{|J_{2N+2}(kR)|}{|J_{N+1}(k\delta)|} \times \sum_{|m|>3N+2} |J_m(k\rho_m)|. \tag{A.13}$$

Indeed, we have $\inf_{n\leq N} |J_{n+1}(k\delta)| = \min(\inf_{n\leq k\delta} |J_{n+1}(k\delta)|, \inf_{k\delta<n\leq N} |J_{n+1}(k\delta)|)$. For $n > k\delta$, $|J_{n+1}(k\delta)|$ as a function of n is decreasing (cf. [27] Eq. (A.6)), and we have $\inf_{n\leq N} |J_{n+1}(k\delta)| = \min(\inf_{n\leq k\delta} |J_{n+1}(k\delta)|, |J_{N+1}(k\delta)|)$. $|J_{n+1}(k\delta)|$ tends to 0, and we have, for sufficiently high orders N, $|J_{N+1}(k\delta)| \leq \inf_{n\leq k\delta} |J_{n+1}(k\delta)|$ and $\inf_{n\leq N} |J_{n+1}(k\delta)| = |J_{N+1}(k\delta)|$. Likewise, as $|m+n| \geq 2N+2$, we have $|J_{m+n}(kR)| \leq |J_{2N+2}(kR)|$.

The Bessel functions have the following asymptotic approximation for large orders:

$$J_n(x) \sim \frac{1}{\sqrt{2\pi n}} \left(\frac{ex}{2n}\right)^n.$$

The series in (A.13) being convergent, the error can be bounded by

$$|u_N - \tilde{u}_N| \leq C'N \left(\frac{(ekR)^2}{2ek\delta} \frac{1}{8(N+1)}\right)^{N+1} \|u\|_{L^2(\Omega)} \tag{A.14}$$

where C' is a positive constant. The error decreases faster than exponentially and, in particular, faster than the error between u and u_N. Similar results can be obtained for the derivatives of u_N, as taking the derivatives will only change the terms appearing in the series in (A.13). Finally, (A.1) is recovered:

$$\|u - \tilde{u}_N\|_{H^q(\Omega)} \leq C \left(\frac{\log N}{N}\right)^{p-q} \|u\|_{H^p(\Omega)}, \tag{A.15}$$

where $\tilde{u}_N$ involves Fourier-Bessel functions of orders up to $4N+2$. While the domain has to be star-convex with respect to a disk, the center of the Fourier-Bessel can be chosen outside of this disk, even outside of the domain of interest. The onset of the asymptotical regime is however likely to be slower than in the original approximation (cf. Eq. (10)), depending on the wavenumber k, the distance between the two centers R and the radius of D.

Acknowledgement

Gilles Chardon is supported by the Austrian Science Fund (FWF) START-project FLAME (Frames and Linear Operators for Acoustical Modeling and Parameter Estimation; Y 551-N13).

[1] Ota DK, Becker T, Sturzenegger T, Chakravarthy SR. Computational study of resonance suppression of open sunroofs. J Fluid Eng-T ASME 1994;116(4):877–882.

[2] Mellet C, Létourneaux F, Poisson F, Talotte C. High speed train noise emission: Latest investigation of the aerodynamic/rolling noise contribution. J Sound Vib 2006;293(3-5):535–546.

[3] Rowley CW, Williams DR. Dynamics and control of high-Reynolds-number flow over open cavities. Annu Rev Fluid Mech 2006;38(1):251–276.

[4] Pelat A, Félix S, Pagneux V. On the use of leaky modes in open waveguides for the sound propagation modeling in street canyons. J Acoust Soc Am 2009;126(6):2864–2872.

[5] Gloerfelt X. Cavity noise. In: VKI Lectures, Aerodynamic noise from wall-bounded flows. Von Karman Institute 2009.

[6] Illingworth SJ, Morgans AS, Rowley CW. Feedback control of flow resonances using balanced reduced-order models. J Sound Vib 2011;330(8):1567–1581.

[7] Ortiz S., Plenier CL, Cobo P. Efficient modeling and experimental validation of acoustic resonances in three-dimensional rectangular open cavities. Appl Acoust 2013;74(7):949–957.

[8] Koch W. Acoustic resonances in rectangular open cavities. AIAA Journal 2005;43(11):2342–2349.

[9] Keller JB, Givoli D. Exact non-reflecting boundary conditions. J Comput Phys 1989;82(1):172–192.

[10] Givoli D. Recent advances in the DtN FE Method. Arch Comput Methods Engrg 1999;6(2):71–116.

[11] Tsynkov SV. Numerical solution of problems on unbounded Domains. A Review. Appl Numer Math 1998;27(4):465–532.

[12] Fox L, Henrici P, Moler C. Approximations and bounds for eigenvalues of elliptic operators. SIAM J Numer Anal 1967;4(1):89–102.

[13] Betcke T, Trefethen LN. Reviving the method of particular solutions. SIAM Rev 2005;47(3):469–491.

[14] Chardon G, Daudet L. Low-complexity computation of plate eigenmodes with Vekua approximations and the method of particular solutions. Comput Mech 2013;52(5):982–992.

[15] Tsai C.C., Young D.L., Chen C.W., Fan C.M. The method of fundamental solutions for eigenproblems in domains with and without interior holes. P Roy Soc Lond A Mat 2006;462 (2069):1443–1466.

[16] Bayliss A, Gunzburger M, Turkel E. Boundary conditions for the numerical solution of elliptic equations in exterior regions, SIAM J Appl Math 1982;42(2):430–451.

[17] Li Y, Cendes ZJ. Modal expansion absorbing boundary conditions for two-dimensional electromagnetic scattering. IEEE Trans Magn 1993;29(2):1835–1838.

[18] Medvinsky M, Turkel E, Hetmaniuk U. Local absorbing boundary conditions for elliptical shaped boundaries. J Comput Phys 2008;227(18):8254–8267.

[19] Engquist B, Majda A. Absorbing boundary conditions for numerical simulation of waves. Proc Natl Acad Sci 1977;74(5):1765–1766.

[20] Halpern L, Trefethen LN. Wide-angle one-way wave equations. J Acoust Soc Am 1988;84(4):1397–1404.

[21] Turkel E, Farhat C, Hetmaniuk U. Improved accuracy for the Helmholtz equation in unbounded domains. Int J Numer Meth Eng 2004;59(15):1963–1988.

[22] Vekua IN. Novye metody rešenija elliptičkikh uravnenij (New Methods for Solving Elliptic Equations). OGIZ, Moskow and Leningrad 1948.

[23] Henrici P. A survey of IN Vekua's theory of elliptic partial differential equations with analytic coefficients. Z Angew Math Phys 1957;8(3):169–203.

[24] Moiola A, Hiptmair A, Perugia I. Plane wave approximation of homogeneous Helmholtz solutions. Z Angew Math Phys 2011;62(5):809–837.

[25] Eisenstat SC. On the rate of convergence of the Bergman-Vekua method for the numerical solution of elliptic boundary value problems. SIAM J Numer Anal 1974;11(3):654–680.

[26] Abramowitz M, Stegun I. Handbook of Mathematical Functions, Dover Publications 1972.

[27] Perrey-Debain E. Plane wave decomposition in the unit disc: Convergence estimates and computational aspects. J Comput Appl Math 2006;193(1):140–156.